Journal of Quality Measurement and Analysis
e-ISSN: 2600-8602
https://doi.org/10.17576/jqma.2103.2025.10

JQMA 21(3) 2025, 161-173
http://www.ukm.my/jqma

EMPLOYING HYPERSINGULAR INTEGRAL EQUATIONS TO OBTAIN STRESS INTENSITY FACTOR FOR TWO SLANTED CRACKS IN THERMOELECTRIC BONDED MATERIALS

(*Menggunakan Persamaan Kamiran Hipersingular untuk Mendapatkan Faktor Keamatan Regangan bagi Dua Retakan Condong dalam Bahan Tercantum Termoelektrik*)

MUHAMMAD HAZIQ IQMAL MOHD NORDIN, KHAIRUM BIN HAMZAH*, ISKANDAR WAINI, NIK MOHD ASRI NIK LONG, NAJIYAH SAFWA KHASHI'IE & AHMAD YUSOF ISMAIL

ABSTRACT

This research focuses on solving hypersingular integral equations (HSIEs) numerically for thermoelectric bonded materials (TEBM) subjected to shear stress and weakened by two slanted cracks. The modified complex variable function (MCVF) method is applied, integrating continuity conditions (CC) for both the electric field effect (EFE) and the displacement electric function (DEF), which are used to formulate the governing HSIEs. Utilizing a curved length coordinate approach, the unknown functions associated with crack opening displacement (COD), as well as constants for current vector field and surface energy load, are expressed in terms of the fracture singularity basis function. These HSIEs are solved numerically using suitable quadrature techniques, with the crack traction as the right-hand term. The solutions for COD, current vector field, and surface energy load are then employed to calculate the dimensionless stress intensity factors (DSIFs), which offer insights into the stability of TEBM with two slanted cracks. Numerical simulations demonstrate that the computed DSIFs at the crack tips are consistent with previous research. Additionally, the results show that DSIFs are significantly affected by factors such as the ratio of elastic constants (ECR), crack geometry, and current vector field coefficients.

Keywords: dimensionless stress intensity factors; bonded materials; hypersingular integral equations; two slanted cracks; thermoelectric

ABSTRAK

Penyelidikan ini mengkaji penyelesaian berangka bagi persamaan kamiran hipersingular (HSIEs) untuk bahan tercantum termoelektrik (TEBM) yang dilemahkan oleh dua retakan condong di bawah tegasan ricih. Kaedah fungsi pembolehubah kompleks yang diubah suai (MCVF) digunakan untuk menangani masalah ini dengan menggabungkan syarat kesinambungan bagi daya elektrik terhasil (EFE) dan fungsi anjakan elektrik (DEF) untuk merumuskan HSIEs. Melalui aplikasi kaedah koordinat panjang lengkung, fungsi tidak diketahui yang berkaitan dengan anjakan pembukaan retakan (COD), serta pemalar bagi ketumpatan arus elektrik dan beban fluks tenaga, diterjemahkan ke dalam rangka kerja fungsi singular punca kuasa dua. Persamaan yang terhasil diselesaikan secara berangka menggunakan formula kuadratur yang sesuai, dengan tarikan retakan sebagai terma sebelah kanan. Fungsi COD, ketumpatan arus elektrik, dan beban fluks tenaga yang dikira digunakan untuk menentukan faktor keamatan regangan tanpa dimensi (DSIF), memberikan pandangan tentang kelakuan kestabilan TEBM yang dilemahkan oleh dua retakan condong. Penyelesaian berangka menunjukkan DSIF pada hujung retakan condong, dengan keserasian yang sangat baik dengan kajian terdahulu. Selain itu, pemerhatian menunjukkan bahawa DSIF dipengaruhi oleh faktor seperti nisbah pemalar keanjalan (ECR), geometri retakan, dan pekali yang berkaitan dengan ketumpatan arus elektrik.

Kata kunci: faktor keamatan regangan tanpa dimensi; bahan tercantum; persamaan kamiran hipersingular; dua retakan condong; termoelektrik

1. Introduction

The reviewed articles highlight the critical role of ensuring the stability and safety of engineering materials, as the presence of cracks can significantly weaken structural integrity. Extensive research has been conducted on the stability behavior of materials and structures under external stresses, encompassing various material types such as infinite (Nik Long & Eshkuvatov 2009; Liu *et al.* 2019), finite (Ghorbanpoor *et al.* 2016; Zhang *et al.* 2019), half-plane (Kebli & Baka 2019; Rangelov & Dineva 2023), and bonded materials (Hamzah *et al.* 2021a; Jiménez-Alfaro & Mantič 2023). These materials exhibit distinct properties, including elasticity (Hamzah & Nik Long 2022; Yadav & Renu 2023), thermoelasticity (Hamzah *et al.* 2021b; Hobiny & Abbas 2023), magnetoelasticity (Xiao *et al.* 2021; Singh 2023), and electrical conductivity (Wang *et al.* 2019; Jiang *et al.* 2020).

Among materials used in manufacturing, thermoelectric materials (TEM) are of particular significance. A finite-size internal crack located arbitrarily within a TEM was analyzed using singular integral equations (SIEs) derived through Fourier and Laplace transforms (Wang *et al.* 2019). The findings indicate that placing the crack at the center leads to a more pronounced concentration of stress near the crack tip. Additionally, the influence of the crack's electrical permeability on energy conversion performance appears to be minimal. To analyze the response of a circular hole accompanied by two unequal cracks within an infinite two-dimensional TEM, the study utilized the complex variable function (CVF) method in conjunction with conformal mapping techniques (Jiang *et al.* 2020). This investigation examined the impact of uniform current vector field and surface energy load on the system. Current vector field represents the flow of electric current through the material, while surface energy load denotes the rate of energy transfer. Both parameters affect the material's response to electrical, thermal, and mechanical loads, influencing crack propagation and overall structural stability. The study showed that variations in the radius of the circular hole and crack lengths influence both the thermoelectric properties and the dimensionless stress intensity factors (DSIFs).

To address two-dimensional scenarios involving a TEM with either an elliptical void or a rigid inclusion, the CVF method was applied alongside conformal mapping techniques (Zhang *et al.* 2017). These configurations were subjected to a uniform electric current field and a surface energy load at an infinite boundary. The investigation indicated that introducing an electric field to the boundary of a hole or rigid body sustains the surface energy load, primarily due to the interplay between Joule heating and the Seebeck effect.

The finite element method was employed to investigate nanoscale cracks in TEM structures under external stress (Sladek *et al.* 2020). This analysis provided valuable insights into how size effects influence variations in Crack Opening Displacements (COD), which measure the relative displacement between crack faces under applied loads and are essential for evaluating crack deformation and predicting propagation. The influence of two collinear interface cracks on the electric potential and temperature profile within a thermoelectric bonded materials (TEBM) system subjected to combined thermal and electrical loads was examined (Jiang & Zhou 2022). Parameters including the length and spacing of the cracks, along with the thickness ratio of the layers, were found to play a crucial role in determining the resulting electric potential and temperature distribution in the TEBM structure. The analysis utilized Laplace equations to assess the DSIFs.

Additionally, the Hankel transform method and integral equation theory were applied to compute DSIFs for a thermo-dielectric medium containing a penny-shaped crack under electrical, thermal, and mechanical loadings (Jiang *et al.* 2023). The investigation explored how the penny-shaped crack and external loading conditions influence the thermal stress fields and behavior of the TEM. SIEs were used to determine the DSIFs for a central crack in a two-dimensional, finite-size TEM, incorporating thermoelectric coupling theories with and without the Thomson effect (Shi *et al.* 2022). The study analyzed how structural size, partially insulated coefficients, and temperature conditions affect the behavior of the TEM.

Integral equations were also employed to characterize the singularity behavior of a ther-

moelectric thin film bonded to an elastic infinite substrate, with DSIFs serving as the primary parameter (Liu *et al.* 2017). The findings underscore the importance of considering film stiffness when evaluating thermal stress levels within thermoelectric films. Finally, the behavior of DSIFs at the tips of an interface crack in TEBM under a remote electric current was examined using CVF (Song *et al.* 2019). The results showed that the effect of current vector field on DSIFs depends on the bonded material parameters, where the electric current may either enhance or diminish the DSIFs based on these parameters.

In the domains of physics and engineering, Hypersingular Integral Equations (HSIEs) are extensively utilized, particularly for analyzing fracture behavior in crack-related problems. This technique offers several strengths over traditional analytical methods, such as higher computational effectiveness, accurate depiction of crack-tip phenomena, versatility in addressing various crack arrangements, and the direct extraction of COD from the obtained solutions (Chan *et al.* 2003; Dutta & Banerjea 2009; Ghorbanpoor *et al.* 2020; Elahi *et al.* 2023a, b). However, certain constraints are still associated with the application of HSIEs. Their formulation and solution processes are typically more intricate than those of simpler methods, such as the boundary element method. Achieving accurate solutions often necessitates careful treatment of crack tip singularities and the application of advanced integration techniques. Nevertheless, HSIEs remain a valuable tool in crack analysis, offering significant insights into the behavior and progression of cracks across diverse engineering applications.

This study aims to compute the numerical solution of DSIFs for the problem of two inclined cracks in TEBM under shear stress using HSIEs and the MCVF method. This work extends the findings of Mohd Nordin *et al.* (2023b), which primarily addressed the formulation and numerical solution of DSIFs for a single crack aligned parallel to the TEBM interface (Mohd Nordin *et al.* 2023a).

To strengthen the foundation of this study, several contemporary works provide valuable insights into the behavior of DSIFs in TEBM and related structures. A study by Mohd Nordin *et al.* (2024) investigated DSIFs for TEBM weakened by an inclined crack using the MCVF method, revealing that DSIFs at crack tips are significantly influenced by the ECR, crack geometry, and current vector field coefficients, thereby enhancing understanding of stability behavior in such materials. Furthermore, research by Benala *et al.* (2023) explored the effect of porosity characteristics on SIFs in spot-welded joints through finite element analysis, demonstrating that factors such as applied loading, crack size, porosity shape and size, and defect interactions play critical roles in fracture mechanics and structural integrity. Additionally, a study by Zhang *et al.* (2024) examined interfacial crack propagation in Bi_2Te_3- based thermoelectric modules under thermal cycling, proposing a fatigue lifetime prediction model based on viscoplastic dissipation energy and validated through experimental and simulation data. These findings provide a broader context for understanding the mechanical response and failure mechanisms in TEBM, reinforcing the relevance and applicability of the current research.

2. Problem Formulation

The stresses (σ_x, σ_y), Electric Field Effect (EFE) (X, Y) and Displacement Electric Function (DEF) (u, v) for a crack in an infinite TEBM are expressed in terms of two complex stress potential functions $\phi(z)$ and $\psi(z)$, and analytic functions for electric $f(z)$ and thermal $g(z)$ fields as follows (Song *et al.* 2019)

$$\sigma_x + \sigma_y = \frac{E\alpha\lambda}{\kappa} f(z)\overline{f(z)} + 2\left[\phi'(z) + \overline{\psi'(z)}\right] \tag{1}$$

$$-Y + iX = \frac{E\alpha\lambda}{4G\kappa} F(z)\overline{f(z)} + \phi(z) + z\overline{\phi'(z)} + \overline{\psi(z)} \tag{2}$$

$$u + iv = + \alpha \int \left[\frac{\lambda}{\kappa} f(z)^2 - \frac{2}{\kappa} g(z)\right] dz + \frac{1}{2G}\left[K\phi(z) - z\overline{\phi'(z)} - \overline{\psi(z)}\right]$$

$$- \frac{E\alpha\lambda}{4G\kappa} F(z)\overline{f(z)} \tag{3}$$

where E is Young's modulus, α is coefficient of thermal expansion, λ is electric conductivity, κ is thermal conductivity, G is shear modulus, $K = (3-\mu)(1+\mu)$, μ is Poisson's ratio, and $F(z) = \int f(z)dz$.

The MCVF for a crack lies in the upper part of TEBM are defined in terms of principal part $(\phi_{1p}(z), \psi_{1p}(z), f_{1p}(z), g_{1p}(z))$ and complementary part $(\phi_{1c}(z), \psi_{1c}(z), f_{1c}(z), g_{1c}(z))$ as follows (Mohd Nordin *et al.* 2023b; Chen & Hasebe 1992)

$$\phi_1(z) = \phi_{1p}(z) + \phi_{1c}(z) \tag{4}$$
$$\psi_1(z) = \psi_{1p}(z) + \psi_{1c}(z) \tag{5}$$
$$f_1(z) = f_{1p}(z) + f_{1c}(z) \tag{6}$$
$$g_1(z) = g_{1p}(z) + g_{1c}(z) \tag{7}$$

whereas the complex stress potential functions for a crack lies in the lower part of TEBM represented by $\phi_2(z)$ and $\psi_2(z)$. By applying the continuity conditions (CC) of EFE (2) and DEF (3) with the help of MCVF (4−7) the following expressions are obtainable

$$\phi_{1c}(z) = \Gamma_1\big(z\overline{\phi'_{1p}}(z) + \overline{\psi_{1p}}(z)\big) + \Gamma_2\overline{F_{1p}}(z)f_{1p}(z) + \Gamma_3\int \overline{f_{1p}}^2(z)dz - \Gamma_4\int \overline{g_{1p}}(z)dz \tag{8}$$

$$\psi_{1c}(z) = \Gamma_5\overline{\phi_{1p}}(z) - z\phi'_{1c}(z) + \Gamma_6\overline{F_{1p}}(z)f_{1p}(z) + \Gamma_7\int \overline{\Omega_{1p}}(z)dz + \Gamma_8\int \overline{f_{1p}}^2(z)dz - \Gamma_9\int \overline{g_{1p}}(z)dz \tag{9}$$

$$\phi_2(z) = \Gamma_{10}\phi_{1p}(z) + \Gamma_{11}F_{1p}(z)\overline{f_{1p}}(z) + \Gamma_{12}F_{1p}(z)\overline{f_{1p}}(z) + \Gamma_7\int \Omega_{1p}(z)dz + \Gamma_8 f_{1p}^2(z)dz - \Gamma_9\int g_{1p}(z)dz \tag{10}$$

$$\psi_2(z) = \Gamma_{13}\big(z\phi'_{1p}(z) + \psi_{1p}(z)\big) - z\phi'_2(z) + \Gamma_{14}F_{1p}(z)f_{1p}(z) + \Gamma_{15}\int {f_{1p}}^2(z)dz - \Gamma_{16}\int g_{1p}(z)dz \tag{11}$$

where $\overline{\phi_{1p}}(z) = \overline{\phi_{1p}(\bar{z})}$, and ECR defined as

$$\Gamma_1 = \frac{G_2 - G_1}{G_1 + G_2K_1}, \quad \Gamma_2 = \frac{\big(2G_2 - 1\big)E_1\alpha_1\lambda_1}{4\kappa_1\big(G_1 + G_2K_1\big)}\left(\frac{\lambda_1 - \lambda_2}{\lambda_1 + \lambda_2}\right)^2,$$
$$\Gamma_3 = \frac{2G_1G_2\alpha_1\lambda_1}{\kappa_1\big(G_1 + G_2K_1\big)}\left(\frac{\lambda_1 - \lambda_2}{\lambda_1 + \lambda_2}\right)^2, \quad \Gamma_4 = \frac{4G_1G_2\alpha_1}{\kappa_1\big(G_1 + G_2\kappa_1\big)}\left(\frac{\kappa_1 - \kappa_2}{\kappa_1 + \kappa_2}\right),$$
$$\Gamma_5 = \frac{G_2K_1 - G_1K_2}{G_1K_2 + G_2}, \quad \Gamma_6 = \frac{E_2\alpha_2\lambda_2\big(2G_1G_2 + G_1K_2\big)}{4G_2\kappa_2\big(G_1K_2 + G_2\big)}\left(\frac{2\lambda_1}{\lambda_1 + \lambda_2}\right)^2,$$
$$\Gamma_7 = \frac{2G_1G_2\alpha_1}{G_1K_2 + G_2}, \quad \Gamma_8 = \frac{2G_1G_2\alpha_2\lambda_2}{\kappa_2\big(G_1K_2 + G_2\big)}\left(\frac{2\lambda_1}{\lambda_1 + \lambda_2}\right)^2,$$
$$\Gamma_9 = \frac{8G_1G_2\alpha_2\kappa_1}{\kappa_2\big(\kappa_1 + \kappa_2\big)\big(G_1K_2 + G_2\big)}, \quad \Gamma_{10} = \frac{(K_1 + 1)G_2}{G_1K_2 + G_2},$$

$$\Gamma_{11}=\frac{E_2\alpha_2\lambda_2(2G_1-1)}{4\kappa_2\big(G_1K_2+G_2\big)}\left(\frac{2\lambda_1}{\lambda_1+\lambda_2}\right)^2,\quad \Gamma_{12}=\frac{G_2E_1\alpha_1\lambda_1(1-2G_1)}{4G_1\kappa_1\big(G_1K_2+G_2\big)},$$
$$\Gamma_{13}=\frac{(K_1+1)G_2}{G_1+G_2K_1},\quad \Gamma_{14}=\frac{\big(K_1+2G_1\big)G_2E_1\alpha_1\lambda_1}{4G_1\kappa_1\big(G_1+G_2K_1\big)}\left(\frac{\lambda_1-\lambda_2}{\lambda_1+\lambda_2}\right)^2,$$
$$\Gamma_{15}=\frac{2G_1G_2\alpha_1\lambda_1\big(1-2G_1\big)}{\kappa_1\big(G_1+G_2K_1\big)}\left(\frac{\lambda_1-\lambda_2}{\lambda_1+\lambda_2}\right)^2,\quad \Gamma_{16}=\frac{4G_1G_2\alpha_1}{\kappa_1\big(G_1+G_2K_1\big)}\left(\frac{\kappa_1-\kappa_2}{\kappa_1+\kappa_2}\right)$$

The normal (N) and tangential (T) components of a crack along the segment $\overline{z,z+dz}$ can be obtained with the derivative in a specified direction of EFE (2) with respect to z as follows

$$\frac{d}{dz}\big\{-Y+iX\big\}=\frac{E\alpha\lambda}{4G\kappa}\left(f(z)\overline{f(z)}+F(z)\overline{f'(z)}\frac{d\bar{z}}{dz}\right)$$
$$+\phi'(z)+\overline{\phi'(z)}+\frac{d\bar{z}}{dz}\left(z\overline{\phi''(z)}+\overline{\psi'(z)}\right)=N+iT \tag{12}$$

where $d\bar{z}/dz=-e^{-2i\theta}$ and θ is the tangential angle to the crack, and the traction $N+iT$ depends on the position of point z and the direction of the segment $d\bar{z}/dz$.

By using superposition principle of the COD function $g_1(t_1)$ along the first crack L_1 and COD function $g_2(t_2)$ along the second crack L_2 to the traction $N+iT$ (12) with the help of the complex stress potential functions (Nik Long & Eshkuvatov 2009), and analytic functions for electric and thermal fields (Song *et al.* 2019), the HSIEs for crack L_1 are obtained as follows (Mohd Nordin *et al.* 2023b)

$$[N(t_{10})+iT(t_{10})]_1=\frac{1}{\pi}\Xint=_{L_1}\frac{g_1(t_1)dt_1}{(t_1-t_{10})^2}+\frac{1}{2\pi}\int_{L_1}M_1(t_1,t_{10})g_1(t_1)dt_1$$
$$+\frac{1}{2\pi}\int_{L_1}M_2(t_1,t_{10})\overline{g_1(t_1)}dt_1+M_3(a_1,t_{10})$$
$$+\frac{1}{\pi}\int_{L_2}\frac{g_2(t_2)dt_2}{(t_2-t_{10})^2}+\frac{1}{2\pi}\int_{L_2}M_1(t_2,t_{10})g_2(t_2)dt_2$$
$$+\frac{1}{2\pi}\int_{L_2}M_2(t_2,t_{10})\overline{g_2(t_2)}dt_2+M_3(a_2,t_{10}). \tag{13}$$

Accordingly, the HSIEs for the crack L_2 can be derived in a similar manner, as shown below.

$$[N(t_{20})+iT(t_{20})]_2=\frac{1}{\pi}\Xint=_{L_2}\frac{g_2(t_2)dt_2}{(t_2-t_{20})^2}+\frac{1}{2\pi}\int_{L_2}M_1(t_2,t_{20})g_2(t_2)dt_2$$
$$+\frac{1}{2\pi}\int_{L_2}E_2(t_2,t_{20})\overline{g_2(t_2)}dt_2+M_3(a_2,t_{20})$$
$$+\frac{1}{\pi}\int_{L_1}\frac{g_1(t_1)dt_1}{(t_1-t_{20})^2}+\frac{1}{2\pi}\int_{L_1}M_1(t_1,t_{20})g_1(t_1)dt_1$$
$$+\frac{1}{2\pi}\int_{L_1}M_2(t_1,t_{20})\overline{g_1(t_1)}dt_1+M_3(a_1,t_{10}). \tag{14}$$

It is important to note that the first integral appearing on the right-hand side of Eqs. (13) and (14) corresponds to a hypersingular integral, which should be interpreted in the sense of a finite-part integral. In solving the HSIEs for two cracks in TEBM, it is well known that the curved

length coordinate method can been used and defined as follows

$$H(s) = \frac{g(t)}{\sqrt{a^2 - s^2}} \tag{15}$$

Then applying the quadrature formulas (Mayrhofer & Fischer 1992; Monegato 1994; Mason & Handscomb 2002; Kythe & Schäferkotter 2004).

The DSIFs F_{A_j} and F_{B_j} at crack tips A_j and B_j respectively, are defined as

$$K_{A_j} = (K_1 - iK_2)_{A_j} = \sqrt{2\pi} \lim_{t \to t_{A_j}} \sqrt{|t - t_{A_j}|} g_1'(t_1) = \sqrt{a\pi} F_{A_j}, \qquad j = 1, 2, \tag{16}$$

$$K_{B_j} = (K_1 - iK_2)_{B_j} = \sqrt{2\pi} \lim_{t \to t_{B_j}} \sqrt{|t - t_{B_j}|} g_2'(t_2) = \sqrt{a\pi} F_{B_j}, \qquad j = 1, 2, \tag{17}$$

where $F_{A_j} = F_{1A_j} + iF_{2A_j}$ and $F_{B_j} = F_{1B_j} + iF_{2B_j}$. A crack propagates when the DSIFs reaches or exceeds its critical limit (Petersen 2013). The material exhibits reduced strength as the DSIFs approaches higher levels (Wang 2003).

3. Numerical Results and Discussions

Consider two slanted cracks in series (Figure 1 (a)) and two slanted cracks in parallel (Figure 1 (b)) in TEBM under shear stress as defined in Figure 1.

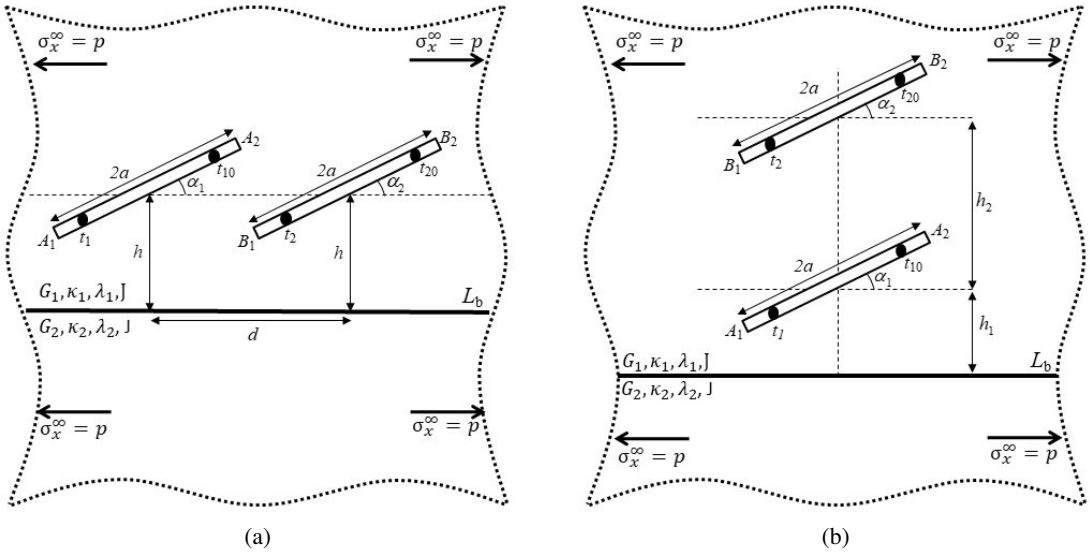

Figure 1: Two slanted cracks in TEBM under shear stress.

Table 1 shows the Mode I (F_1) and Mode II (F_2) DSIFs for two slanted cracks in series in TEBM under shear stress when $\alpha_1 = \alpha_2 = 90°$, $2a/h = 1.8$, $G_2/G_1 = 1.0$ and $J = U = 0$ at crack tips A_1 and A_2 (Figure 1 (a)). The DSIFs at crack tips A_1 and A_2 are found to be identical to those at tips B_1 and B_2, respectively. The outcomes of this study align well with the findings reported in Hamzah *et al.* (2019), Denda & Dong (1997), and Murakami (1987).

Consider two slanted cracks defined in Figure 1 (a) when $\alpha_1 = 90°$, $h = a/0.9$ and $U = 0$ for $J = 0$ (Blue), $J = 20$ (Red) and $J = 60$ (Black). Figure 2 presents the Mode I (F_1) DSIFs versus α_2 at all crack tips. It has been identified that changes in α_2 have little effect on F_1 at crack tips A_1 and A_2. However, when α_2 exceeds $30°$, F_1 at tips B_1 and B_2 exhibits a

Table 1: DSIFs for two slanted cracks in series in TEBM when $\alpha_1 = \alpha_2 = 90^\circ$, $2a/h = 1.8$, $G_2/G_1 = 1.0$ and $J = U = 0$.

DSIFs	$2a/d$							
	0.2	0.4	0.6	0.8	1.0	2.0	3.0	5.0
F_{1A_1}*	0.9858	0.9505	0.9092	0.8722	0.8431	0.7734	0.7463	0.7215
F_{1A_1} **	0.9857	0.9505	–	0.8722	0.8431	0.7734	–	0.7215
F_{1A_1} ***	0.9870	0.9517	–	0.8732	0.8440	0.7746	–	0.7129
F_{1A_1} ****	0.9855	0.9508	–	0.8727	0.8319	0.7569	–	0.6962
F_{1A_2}*	0.9858	0.9506	0.9092	0.8722	0.8431	0.7734	0.7463	0.7215
F_{1A_2} **	0.9857	0.9505	–	0.8722	0.8431	0.7734	–	0.7215
F_{2A_1}*	0.0014	0.0094	0.0246	0.0431	0.0611	0.1165	0.1405	0.1633
F_{2A_1} **	0.0014	0.0094	–	0.0431	0.0611	0.1165	–	0.1633
F_{2A_2}*	−0.0014	−0.0094	−0.0246	−0.0431	−0.0611	−0.1165	−0.1405	−0.1633
F_{2A_2} **	−0.0014	−0.0094	–	−0.0431	−0.0611	−0.1165	–	−0.1633

*Present study
**Hamzah *et al.* (2019)
***Denda & Dong (1997)
****Murakami (1987)

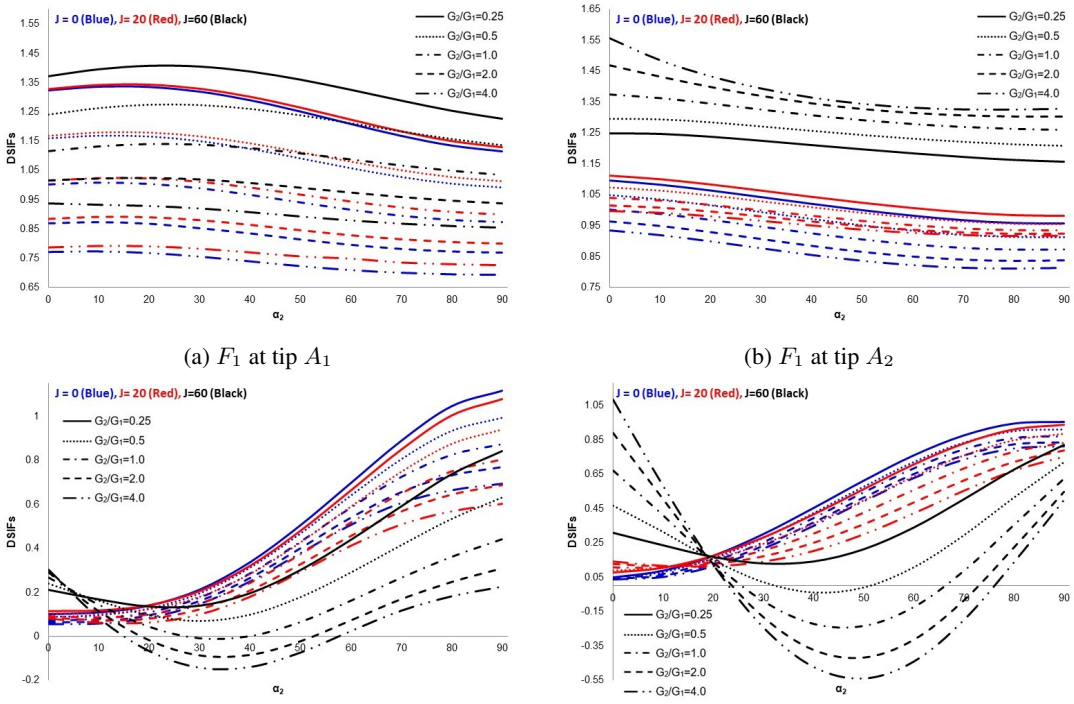

(a) F_1 at tip A_1

(b) F_1 at tip A_2

(c) F_1 at tip B_1

(d) F_1 at tip B_2

Figure 2: Mode I (F_1) DSIFs versus α_2 at all crack tips (Figure 1 (a)).

noticeable amplification. As the ratio G_2/G_1 becomes more pronounced, a reduction in F_1 is evident across all crack tips. In contrast, higher values of J correspond to elevated F_1 at crack tips A_1 and A_2, while F_1 at tips B_1 and B_2 tends to diminish. Figure 3 illustrates the Mode II (F_2) DSIFs as a function of α_2 at all crack tips. It is observed that F_2 rises at crack tips

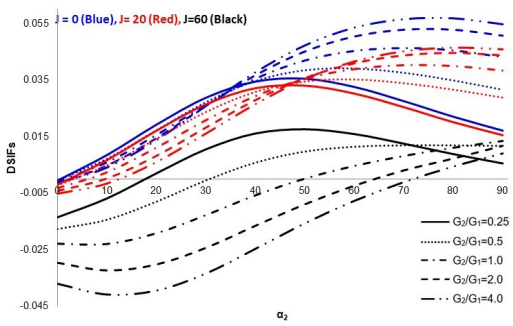

(a) F_2 at tip A_1

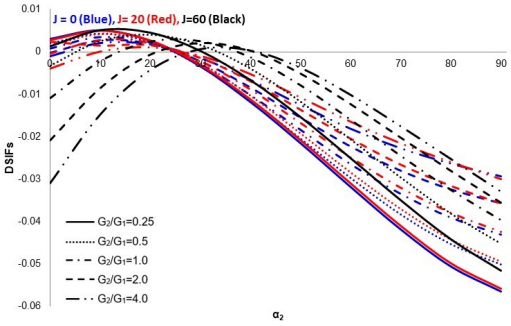

(b) F_2 at tip A_2

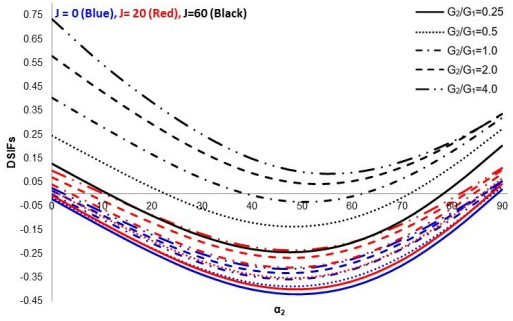

(c) F_2 at tip B_1

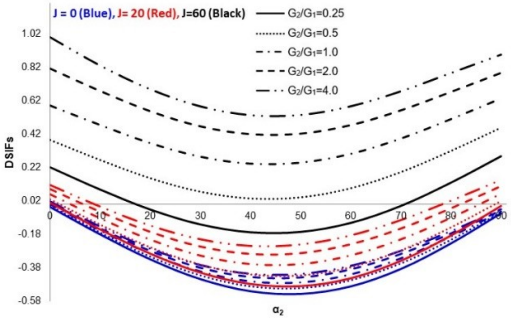

(d) F_2 at tip B_2

Figure 3: Mode II (F_2) DSIFs versus α_2 at all crack tips (Figure 1 (a)).

A_1 but falls at A_2 when $\alpha_2 > 30°$, while at crack tips B_1 and B_2, F_2 reduces for $\alpha_2 < 45°$. For higher values of G_2/G_1, F_2 becomes more pronounced at crack tips B_1 and B_2. Similarly, as J grows, F_2 becomes more significant at B_1 and B_2, but at A_1 and A_2, a reduction in F_2 is noted. The numerical results suggest that larger α_2 and J lvalues are associated with weakened material strength, implying a greater vulnerability to crack propagation and structural failure under enhanced shear loading and crack misalignment. This highlights the need for careful design to minimize crack angles and loading intensity to maintain structural integrity. Conversely, an increase in the ECR G_2/G_1 enhances material stability by improving resistance to crack growth and fracture. This suggests that selecting materials with higher stiffness contrast between bonded layers can effectively enhance fracture toughness and overall durability in thermoelectric bonded structures under operational stress.

Consider two slanted cracks in parallel within a TEBM under shear stress, as shown in Figure 1 (b), where $\alpha_1 = \alpha_2$, $h_1 = a/0.9$, $h_1 + h_2 = 3.5a$, and $U = 0$ for $J = 0$ (Blue), $J = 10$ (Red) and $J = 20$ (Black). Figure 4 illustrates the Mode I (F_1) DSIFs as a function of α_1 at all crack tips. The results show that as α_1 becomes larger, F_1 becomes more pronounced at all crack tips. When G_2/G_1 rises, a reduction in F_1 occurs at crack tips A_1 and A_2; however, at crack tips B_1 and B_2, F_1 becomes more significant for $J = 0$ (Blue) and $J = 10$ (Red), and and for $J = 0$ (Black), it becomes less. As J grows, F_1 intensifies at all crack tips. Figure 5 shows the Mode II (F_2) DSIFs as a function of α_1 at all crack tips. It is observed that for $\alpha_1 > 45°$, F_2 becomes more significant at all crack tips. When G_2/G_1 rises, F_2 becomes more pronounced at crack tips A_1, B_1 and B_2; however, at crack tip A_2, F_2 is reduced for $J = 20$ (Black), and becomes larger for $J = 0$ (Blue) and $J = 10$ (Red). As J grows, F_2 reduces at crack tips A_1, A_2 and B_1, but at crack tip B_2, F_2 becomes more pronounced. The numerical outcomes suggest that increasing in α_1 and J reduces material strength by promoting higher stress concentration at crack tips, increasing the likelihood of crack propagation and structural failure under shear loading. This implies that minimizing crack inclination and loading intensity is

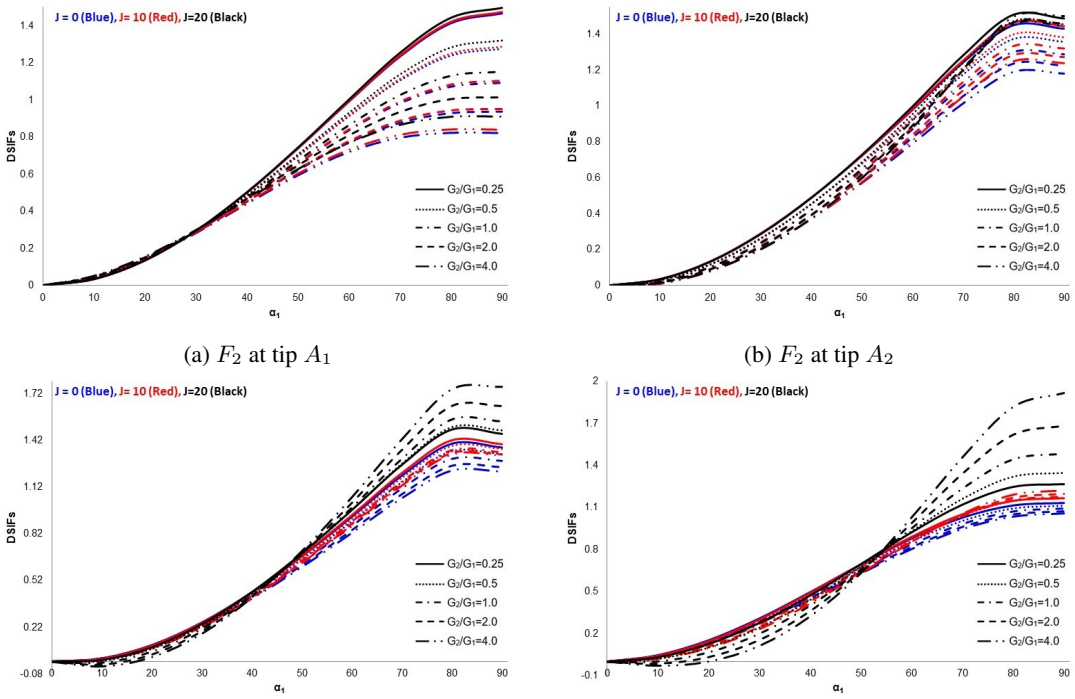

(a) F_2 at tip A_1

(b) F_2 at tip A_2

(c) F_2 at tip B_1

(d) F_2 at tip B_2

Figure 4: Mode I (F_1) DSIFs versus α_1 at all crack tips (Figure 1 (b)).

critical for maintaining structural integrity in TEBM. On the other hand, a higher ECR (G_2/G_1) enhances material stability by increasing resistance to crack growth, thereby improving fracture toughness. This indicates that selecting materials with higher stiffness contrast between bonded layers can enhance the overall durability and performance of TEBM under operational stress.

4. Conclusion

In this investigation, HSIEs have been utilized to conduct a numerical analysis of DSIFs for two slanted cracks in for TEBM under shear stress. Building upon prior work that primarily focused on the mathematical formulation of similar problems (Mohd Nordin *et al.* 2023b), this study introduces significant advancements. A key contribution is the innovative application of the MCVF method, traditionally employed for crack problems in bonded materials, to specifically analyze two slanted cracks in TEBM. This approach utilizes HSIEs, with critical variables including the COD, current vector field, and surface energy load between crack tips. The comprehensive solution derived for the HSIEs effectively captures the complexity of two slanted cracks in TEBM. Numerical results reveal that the DSIFs are influenced by factors such as the ECR, current vector field, crack geometries, and the proximity of the crack to the boundary. These insights are crucial for understanding how such factors affect the mechanical performance and reliability of TEBM.

Beyond theoretical contributions, the findings have practical implications for engineering applications. The results provide a valuable framework for designing TEBM with enhanced durability and reliability under mechanical and thermal stress. Engineers can use the insights from this study to optimize material configurations, predict failure modes, and improve safety margins in applications such as energy harvesting devices, aerospace systems, and microelectronics. The methodology could also be integrated into material testing protocols and quality control processes to assess and mitigate crack propagation risks.

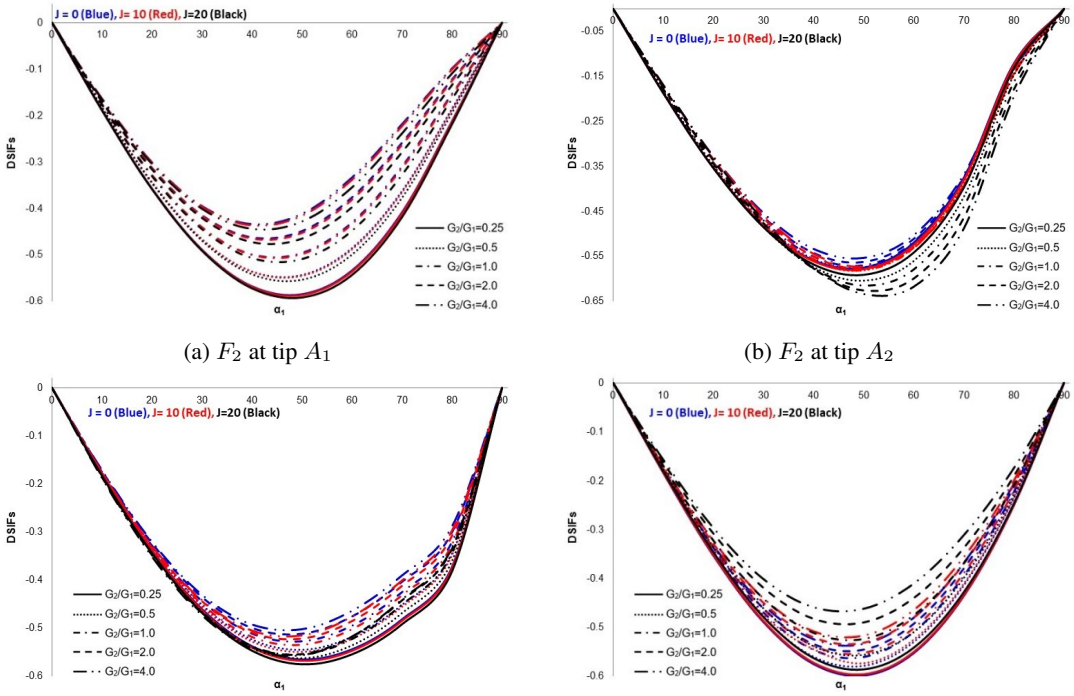

(a) F_2 at tip A_1

(b) F_2 at tip A_2

(c) F_2 at tip B_1

(d) F_2 at tip B_2

Figure 5: Mode II (F_2) DSIFs versus α_1 at all crack tips (Figure 1 (b)).

This study also opens up several promising directions for future research. Potential extensions include investigating cohesive crack models, analyzing cracks at material interfaces, exploring the effects of inclusions on crack behavior, and addressing three-dimensional crack problems in TEBM. Such efforts will further bridge the gap between theoretical models and practical applications, ultimately enhancing the performance and reliability of advanced bonded materials in diverse engineering contexts.

Acknowledgement

The authors gratefully acknowledge the continuous support provided by Universiti Teknikal Malaysia Melaka (UTeM). Appreciation is also extended to the editor and anonymous reviewers for their thoughtful feedback and suggestions, which have greatly contributed to enhancing the quality of this manuscript.

References

Benala I., Zouambi L., Bouafia F., Serier B. & Hayat S.S. 2023. Effect of porosity shape, size and distribution on stress intensity factors in spot welded joints: A finite element study. *Annales de Chimie Science des Matériaux* **47**(3): 4.

Chan Y.S., Fannjiang A.C. & Paulino G.H. 2003. Integral equations with hypersingular kernels—-theory and applications to fracture mechanics. *International Journal of Engineering Science* **41**(7): 683–720.

Chen Y.Z. & Hasebe N. 1992. Stress-intensity factors for curved circular crack in bonded dissimilar materials. *Theoretical and Applied Fracture Mechanics* **17**(3): 189–196.

Denda M. & Dong Y.F. 1997. Complex variable approach to the BEM for multiple crack problems. *Computer Methods in Applied Mechanics and Engineering* **141**(3-4): 247–264.

Dutta B. & Banerjea S. 2009. Solution of a hypersingular integral equation in two disjoint intervals. *Applied Mathematics Letters* **22**(8): 1281–1285.

Elahi M.R., Mahmoudi Y., Shamloo A.S. & Rad M.J. 2023a. A novel collocation method for numerical solution of hypersingular integral equation with singular right-hand function. *Advances in Mathematical Physics* **2023**(1): 5845263.

Elahi M.R., Mahmoudi Y., Shamloo A.S. & Rad M.J. 2023b. On projection method for numerical solution of hypersingular integral equations of the first kind combined with quadrature methods. *Physica Scripta* **98**(4): 045229.

Ghorbanpoor R., Nik Long N.M.A. & Eshkuvatov Z.K. 2016. Formulation for multiple curved crack problem in a finite plate. *Malaysian Journal of Mathematical Sciences* **10**: 253–263.

Ghorbanpoor R., Saberi-Nadjafi J., Nik Long N.M.A. & Erfanian M. 2020. Stress intensity factor for multiple cracks in an infinite plate using hypersingular integral equations. *Computational Methods for Differential Equations* **8**(1): 69–84.

Hamzah K.B. & Nik Long N.M.A. 2022. Effect of mechanical loadings on two unequal slanted cracks length in bi-materials plate. *Malaysian Journal of Mathematical Sciences* **16**(2): 185–197.

Hamzah K.B., Nik Long N.M.A., Senu N. & Eshkuvatov Z.K. 2019. Stress intensity factor for multiple cracks in bonded dissimilar materials using hypersingular integral equations. *Applied Mathematical Modelling* **73**: 95–108.

Hamzah K.B., Nik Long N.M.A., Senu N. & Eshkuvatov Z.K. 2021a. Numerical solution for crack phenomenon in dissimilar materials under various mechanical loadings. *Symmetry* **13**(2): 235.

Hamzah K.B., Nik Long N.M.A., Senu N. & Eshkuvatov Z.K. 2021b. Numerical solution for the thermally insulated cracks in bonded dissimilar materials using hypersingular integral equations. *Applied Mathematical Modelling* **91**: 358–373.

Hobiny A. & Abbas I.A. 2023. A study on the thermoelastic interaction in two-dimension orthotropic materials under the fractional derivative model. *Alexandria Engineering Journal* **64**: 615–625.

Jiang D., Luo Q.H., Liu W. & Zhou Y.T. 2020. Thermoelectric field disturbed by two unequal cracks adjacent to a hole in thermoelectric materials. *Engineering Fracture Mechanics* **235**: 107163.

Jiang D. & Zhou Y.T. 2022. Role of crack length, crack spacing and layer thickness ratio in the electric potential and temperature of thermoelectric bi-materials systems. *Engineering Fracture Mechanics* **259**: 108170.

Jiang D., Zhou Y.T. & Li F. 2023. The thermo-dielectric medium crack model with penny shape in thermoelectric materials. *Acta Mechanica* **234**(9): 3779–3800.

Jiménez-Alfaro S. & Mantič V. 2023. Crack tip solution for mode III cracks in spring interfaces. *Engineering Fracture Mechanics* **288**: 109293.

Kebli B. & Baka Z. 2019. Annular crack in an elastic half-space. *International Journal of Engineering Science* **134**: 117–147.

Kythe P.K. & Schäferkotter M.R. 2004. *Handbook of Computational Methods for Integration*. Boca Raton, FL: Chapman & Hall/CRC.

Liu Y., Wang B.L. & Zhang C. 2017. Mechanical model for a thermoelectric thin film bonded to an elastic infinite substrate. *Mechanics of Materials* **114**: 88–96.

Liu Z.X., Xu W., Yu Y. & Wu X.R. 2019. Weight functions and stress intensity factors for two unequal-length collinear cracks in an infinite sheet. *Engineering Fracture Mechanics* **209**: 173–186.

Mason J.C. & Handscomb D.C. 2002. *Chebyshev Polynomials*. Boca Raton, FL: Chapman & Hall/CRC.

Mayrhofer K. & Fischer F.D. 1992. Derivation of a new analytical solution for a general two-dimensional finite-part integral applicable in fracture mechanics. *International Journal for Numerical Methods in Engineering* **33**(5): 1027–1047.

Mohd Nordin M.H.I., Hamzah K.B., Khashiie N.S., Waini I., Zainal N.A. & Sayed Nordin S.K. 2023a. Derivation of hyper-singular integral equations for thermoelectric bonded materials featuring a crack parallel to interface. *Mathematical Modeling and Computing* **10**(4): 1230–1238.

Mohd Nordin M.H.I., Hamzah K.B., Khashi'ie N.S., Waini I., Nik Long N.M.A. & Fitri S. 2023b. Formulation for multiple cracks problem in thermoelectric-bonded materials using hypersingular integral equations. *Mathematics* **11**(14): 3248.

Mohd Nordin M.H.I., Hamzah K.B., Nik Long N.M.A., Khashiie N.S., Waini I., Zainal N.A. & Sayed Nordin S.K. 2024. Stress intensity factors for thermoelectric bonded materials weakened by an inclined crack. *Journal of Advanced Research in Applied Mechanics* **113**(1): 52–62.

Monegato G. 1994. Numerical evaluation of hypersingular integrals. *Journal of Computational and Applied Mathematics* **50**(1-3): 9–31.

Murakami Y. 1987. *Handbook of Stress Intensity Factors*. Oxford, UK: Pergamon Press.

Nik Long N.M.A. & Eshkuvatov Z.K. 2009. Hypersingular integral equation for multiple curved cracks problem in plane elasticity. *International Journal of Solids and Structures* **46**(13): 2611–2617.

Petersen R.C. 2013. Accurate critical stress intensity factor Griffith crack theory measurements by numerical techniques. *SAMPE Journal* **2013**: 737.

Rangelov T. & Dineva P. 2023. BIEM via graded piezoelectric half-plane Green's function for wave scattering by curvilinear cracks. *Archive of Applied Mechanics* **93**(9): 3683–3696.

Shi P., Qin W., Li X. & Xie J. 2022. Thermoelectric conversion efficiency of a two-dimensional thermoelectric plate of finite-size with a center crack. *Acta Mechanica* **233**(11): 4785–4803.

Singh A.K. 2023. Anisotropy and magnetoelasticity effects on the propagation of the SH-wave-induced semi-infinite crack in a magnetoelastic orthotropic medium. *Physica Scripta* **98**(11): 115247.

Sladek J., Sladek V., Repka M. & Schmauder S. 2020. Crack analysis of nano-sized thermoelectric material structures. *Engineering Fracture Mechanics* **234**: 107078.

Song K., Song H.P., Schiavone P. & Gao C.F. 2019. Electric current induced thermal stress around a bi-material interface crack. *Engineering Fracture Mechanics* **208**: 1–12.

Wang P., Wang B.L. & Wang K.F. 2019. Dynamic response of cracked thermoelectric materials. *International Journal of Mechanical Sciences* **160**: 298–306.

Wang T.C. 2003. Fundamentals of interface mechanics. In Milne I., Ritchie R.O. & Karihaloo B. (eds.). *Comprehensive Structural Integrity*: 89–135. Oxford, UK: Pergamon.

Xiao J., Feng G., Su M., Xu Y. & Zhang F. 2021. Fracture analysis on periodic radial cracks emanating from a nanohole with surface effects in magnetoelectroelastic materials. *Engineering Fracture Mechanics* **258**: 108115.

Yadav R.P. & Renu 2023. On the dynamic mode-III crack in the elastic continuum consisting of sandy properties. *Physica Scripta* **98**(10): 105203.

Zhang A.B., Wang B.L., Wang J. & Du J.K. 2017. Two-dimensional problem of thermoelectric materials with an elliptic hole or a rigid inclusion. *International Journal of Thermal Sciences* **117**: 184–195.

Zhang J., Qu Z., Liu W. & Wang L. 2019. Automated numerical simulation of the propagation of multiple cracks in a finite plane using the distributed dislocation method. *Comptes Rendus Mécanique* **347**(3): 191–206.

Zhang Y., He H., Niu C., Wu Y., Liu M., Liu S., Liu Y., Wu C. & Rong M. 2024. Interfacial crack growth-based fatigue lifetime prediction of thermoelectric modules under thermal cycling. *ACS Applied Materials & Interfaces* **16**(1): 1137–1147.

Fakulti Teknologi dan Kejuruteraan Industri dan Pembuatan,
Universiti Teknikal Malaysia Melaka,
Hang Tuah Jaya, 76100 Durian Tunggal,
Melaka, MALAYSIA
E-mail: haziqiqmal77@gmail.com, khairum@utem.edu.my, iskandarwaini@utem.edu.my*

Department of Mathematics,
Faculty of Science,
Universiti Putra Malaysia,
43400 UPM Serdang,
Selangor, MALAYSIA
E-mail: nmasri@upm.edu.my

Fakulti Teknologi dan Kejuruteraan Mekanikal,
Universiti Teknikal Malaysia Melaka,
Hang Tuah Jaya, 76100 Durian Tunggal,
Melaka, MALAYSIA
E-mail: najiyah@utem.edu.my

Faculty of Industrial Technology,
Institut Teknologi Adhi Tama Surabaya,
Jawa Timur 60117,
INDONESIA
E-mail: yusuf@itats.ac.id

Received: 7 September 2024
Accepted: 13 May 2025

*Corresponding author